Determination of Breakdown Voltage Characteristics of 1'100 kV disconnector for modeling of VFTO in Gas-Insulated Switchgear

Marcin Szewczyk, *Senior Member, IEEE*, Maciej Kuniewski, *Member, IEEE*, Wojciech Piasecki, *Member, IEEE*, Marek Florkowski, *Senior Member, IEEE*, and Ueli Straumann, *Senior Member, IEEE*

***Abstract*— This paper presents a method for determination of Breakdown Voltage Characteristics (BDV) of Gas-Insulated Switchgear (GIS) disconnector. The method is applicable for modeling of Very Fast Transient Overvoltages (VFTO) that are generated during the disconnector opening and closing operations. The method is based on full-scale measurements, as typically performed during the disconnector development- and/or type- tests. The method is first presented in a simplified, illustrative setting, and then applied for the full-scale measurement results obtained for an 1'100 kV disconnector design. The BDV determined is then applied for two 1'100 kV test set-ups as recently reported for the Wuhan (China) station. Selected test cases are simulated, analyzed and validated with the use of the multi-spark modeling approach, with two BDV characteristics implemented: the *Non-linear BDV* obtained with the method presented here applied for the measurement results on the example 1'100 kV disconnector, and the *Linear BDV* reported in the literature for 1'100 kV disconnector used in the Wuhan GIS station.**

***Index Terms*— Very Fast Transient Overvoltages (VFTOs), Gas-Insulated Switchgear (GIS), disconnector switch (DS), modelling, simulations, transients, switching**

I. Introduction

MODELING of Very Fast Transient Overvoltages (VFTO) in Gas-Insulated Switchgear (GIS) is essential for the GIS disconnector design work, for supporting the disconnector full-scale type testing, and for supporting a decision on application, selection, and dimensioning of the VFTO damping solutions. These aspects require detailed and accurate modeling of the entire disconnector operation process, which can be satisfied when using the multi-spark approach, where the entire operation of the GIS disconnector is modeled as opposed to the state-of-the-art single-spark approach where only a single VFTO occurrence can be analyzed.

M. Szewczyk, W. Piasecki, M. Florkowski are with ABB Corporate Research Center, 31-038 Krakow, Starowislna 13A, Poland (e-mail: marcin.szewczyk@pl.abb.com, wojciech.piasecki@pl.abb.com, marek. florkowski@pl.abb.com).

M. Kuniewski is with AGH University of Science and Technology, Department of Electrical and Power Engineering, al. Mickiewicza 30, 30-059 Kraków, Poland (e-mail: maciej.kuniewski@agh.edu.pl).

U. Straumann is with ABB Switzerland Ltd., Zürich 8050, Switzerland (e-mail: ulrich.straumann@ch.abb.com).

Corresponding author: M. Szewczyk (e-mail: marcin.szewczyk@pl.abb. com).

Color versions of one or more of the figures in this paper are available online at http://ieeexplore.ieee.org

A. Breakdown Voltage Characteristics

A critical aspect of the GIS disconnector modeling with the multi-spark approach is to accurately determine and implement the model of the disconnector Breakdown Voltage Characteristics (BDV). The BDV characterizes the dielectric strength of the disconnector contact system during the disconnector opening and closing operations. It is thus a major factor for determining voltage conditions which govern repetitive ignitions of gas breakdown (sparks) occurring in the disconnector contact gap. The spark ignitions occur at the time instances when the voltage across the disconnector contact system exceeds the instantaneous BDV value. The BDV has thus the major impact on the VFTO amplitude, as well as on other parameters characterizing disconnector operation, such as Trapped Charge Voltage (TCV), sparking time, and total number of sparks.

On the other hand, the BDV is strongly related to the disconnector design, specifically to the disconnector contact system design (e.g. electric field grading elements), insulation media characteristics (e.g. SF_6 gas pressure), and operating characteristics of the disconnector's moving contact (e.g. moving contact speed).

B. Disconnector design perspective

For EHV and UHV class GIS, the VFTO may become a design factor due to the lowered ratio between the equipment rated- and withstand-voltage levels [12]. The overall design of the GIS disconnector is a compromise between several factors, among which the quantities outlined in Section I.A are often investigated throughout simulations and measurements. As an example, it is known from e.g. [1], [2] that for the disconnector opening operation, the BDV with the decreased rise time causes that the average values of the TCV distributions are shifted towards lowered values. This leads to significant decrease of the VFTO amplitudes during the subsequent closing operation, and consequently makes the worst-case scenario of $\mathrm{TCV} = -1$ p.u. (as used in the standardized type-testing procedures recommended by IEC Std. [3]) highly unlikely [1], [2], [4]. In practice, the BDV slope is often being decreased by means of reducing the disconnector's moving contact speed [1], [2], [4]. As a consequence, the arcing time and the number of sparks are increased, which can lead to higher thermal requirements for the contact system, especially under bus-transfer operations.

C. 1100 kV test set-ups used as a reference in this paper

In order to analyze the above mentioned quantities, full-scale test set-ups are being developed by GIS manufacturers and grid operators. Three test set-ups of that kind are outlined below as being referenced in the present paper, providing measurement data for presentation and validation of the methodology presented here.

Since 2008, development tests have been conducted on 1'100 kV disconnectors for piloting the Ultra-High Voltage (UHV) GIS development, such as for Jingmen 1'100 kV station in China [5]. The distributions of VFTO, TCV, sparking time, and total number of sparks are being measured for selected disconnector designs. As an example, in 2008 two operating speeds of the disconnector's moving contact were selected as $0.39\ \mathrm{m/s}$ and $0.54\ \mathrm{m/s}$ for both the opening and the closing operations. Approximately 100 disconnector operations were performed for each disconnector design and each of the moving contact speed. Based on these results, investigations of the disconnector design impact on different aspects of VFTO were reported e.g. in [1], [4], [6].

In 2009, State Grid Corporation China (SGCC) has established two test set-ups in Wuhan 1'100 kV station in China. Based on these test set-ups, several papers have been recently published (e.g. [2], [7]-[9]), where the impact of the disconnector design on different aspects of VFTO was analyzed for the disconnectors with different operating speeds. In [2], [7] the moving contact speed was $0.54\ \mathrm{m/s}$ for both the opening and the closing operation; in [9] the speeds for the opening and the closing operations were $0.71\ \mathrm{m/s}$ and $2.10\ \mathrm{m/s}$ respectively; in [2], [7], [9] the speeds for the opening and the closing operations were $1.70\ \mathrm{m/s}$ and $2.50\ \mathrm{m/s}$ respectively. Different aspects of VFTO were analyzed, including distributions of VFTO, TCV, sparking time, and total number of sparks [2], [7], [9]. In [2], [9] the linear BDV characteristics was assumed for modeling and simulations.

D. Paper overview

This paper presents a method for determination of BDV characteristics of the GIS disconnector, for modeling of the VFTO in GIS. The method of the BDV determination is based on full-scale measurements involving the entire opening and closing operations of the GIS disconnector. For the purpose of the method presentation and validation, selected measurement results are used in this paper from the three 1'100 kV test set-ups as outlined in Section I.C above.

The paper is organized as follows: Section I introduces basic information on the BDV and gives design perspective on the applicability of the work presented.

In Section II, the method of BDV determination is presented with the use of a simplified, illustrative simulation set-up. Then, the method is applied to determine the BDV based on the full-scale measurement results of an example of 1'100 kV disconnector as used by ABB at development tests. Example simulation results are outlined in Section II to confirm validation of the BDV determined. The BDV determined in Section II is further referred in this paper as a *Non-linear BDV*. A BDV reported in [8] (referred further in this paper as a *Linear BDV*) was further benchmarked with the *Non-Linear BDV*, providing reference for analyses presented in Section III.

In Section III, both BDVs (*Non-linear* and *Linear*) are implemented in the multi-spark approach. Selected simulation results are presented to demonstrate the approach applicability for VFTO analyses. Disconnector operations were modeled according to the multi-spark approach applied for the two test set-ups of Wuhan 1'100 kV GIS station. The Wuhan test set-ups were modeled according to the description reported in [2], [7]-[9].

Section IV presents comparison of the selected simulation results to the measurement results as reported for Wuhan station in [7].

Section V offers final conclusions.

II. Determination of Breakdown Voltage Characteristics based on Full-Scale Measurements

A. Method description

During the disconnector operation, repetitive gas breakdown (sparks) occur in the disconnector contact gap at the time instances t_i when the voltage across the disconnector contact system $u_{\mathrm{d}}(t)$ exceeds the instantaneous value of the BDV. The voltage $u_{\mathrm{d}}(t)$ is defined by the instantaneous values of the voltages at the disconnector source- $u_{\mathrm{S}}(t)$ and load- $u_{\mathrm{L}}(t)$ sides. For the time instance of the sparks ignitions t_i the voltage $u_{\mathrm{d}}(t_i)$ is given by:

$$u_{\mathrm{d}}(t_i) = u_{\mathrm{S}}(t_i) - u_{\mathrm{L}}(t_i) \tag{1}$$

Since the BDV depends on the $u_{\mathrm{d}}(t)$ polarity (which is due to the typically asymmetric design of the disconnector contact system), the BDV is thus defined by the positive- $u^{+}_{\mathrm{BDV}}(t)$ and the negative- $u^{-}_{\mathrm{BDV}}(t)$ breakdown voltages. The $u^{+}_{\mathrm{BDV}}(t)$ and $u^{-}_{\mathrm{BDV}}(t)$ describe the withstand voltage instantaneous values for the positive and the negative voltage $u_{\mathrm{d}}(t)$ respectively. The sparks are thus being ignited at the time instances t_i according to the voltage conditions given by the following formula:

$$u_{\mathrm{d}}(t_i) \geq u^{+}_{\mathrm{BDV}}(t_i) \ \text{ or } \ u_{\mathrm{d}}(t_i) \leq u^{-}_{\mathrm{BDV}}(t_i) \tag{2}$$

where $u_{\mathrm{d}}(t_i)$ is the voltage across the disconnector contact system given by (1), and $u^{+/-}_{\mathrm{BDV}}(t_i)$ are the breakdown voltages for the positive and the negative voltage polarity respectively; for the time instances t_i of the sparks ignitions.

The disconnector design-specific BDV, specified by the breakdown voltages $u^{+/-}_{\mathrm{BDV}}(t_i)$, can be thus determined by performing operation of the disconnector, during which the time instances t_i of the sparks ignitions are recorded together with the associated values of the voltage $u_{\mathrm{d}}(t_i)$. These quantities are typically measured during the standardized type-test procedures, such as recommended by IEC Std. [3].

B. Determination of BDV in simplified simulation set-up

Fig. 1 shows a simplified simulation set-up used in this section for illustrating of the BDV determination method. Its structure is similar to that of the one according to the IEC type-testing procedure [3] (see also Section II.C and Fig. 5),

with the only difference that the models of the GIS busbars are here simplified to the lumped equivalent capacitances C_1 and C_2 (see Fig. 5). The AC voltage source generates the voltage on the disconnector source-side, which is of 1.1 p.u. amplitude (where 1 p.u. $= U_r\sqrt{2/3}$; U_r is rated voltage) and 50/60 Hz frequency. For modeling of the disconnector operation, the multi-spark approach was employed, modeling the entire operation of the disconnector.

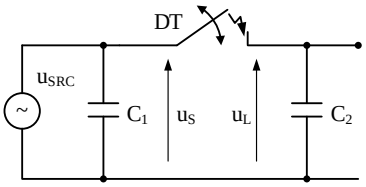

Fig. 1 Simplified simulation set-up used for illustration of BDV determination method: $u_{SRC} = 1.1$ p.u. – source voltage, u_S and u_L – disconnector source- and load-side voltages respectively, DT – operated disconnector "under test", $C_1 = 3.3$ nF – source-side capacitance, $C_2 = 2$ nF – capacitive load; distributed models of GIS busbars are simplified with the lumped capacitances.

Fig. 2 shows a simplified BDV, assumed for illustrative purposes in this section, in a form of two three-segment lines, for the positive $u^+_{BDV}(t)$ (in blue color) and the negative $u^-_{BDV}(t)$ (in red color) polarities of the voltage $u_d(t)$. In Fig. 2, the simulated voltage $u_d(t)$ is depicted for different number n of disconnector opening operations ($n = 2$ in Fig. 2a and $n = 5$ in Fig. 2b), where each operation was conducted for different phase at which the disconnector's moving contact separation started.

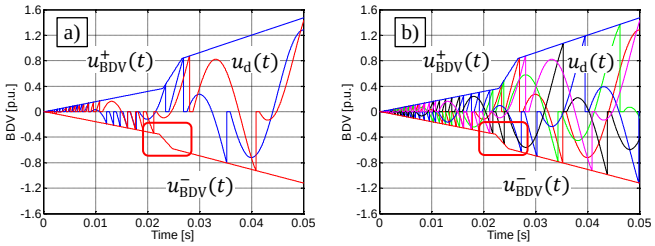

Fig. 2 BDV characteristics assumed for the method illustration (three-segment lines): positive $u^+_{BDV}(t)$ (blue) and negative $u^-_{BDV}(t)$ (red) breakdown voltages; voltage $u_d(t)$ simulated in set-up shown in Fig. 1 for the BDV assumed, for: $n = 2$ (a) and $n = 5$ disconnector opening operations.

The assumed illustrative profile of the BDV introduces a discontinuity at the time range between 0.02 s and 0.03 s. The discontinuity is introduced for the purpose of providing diverse conditions for the method presentation. The remaining parts of BDV corresponds to the moving contact speed which is approximately 5 times higher than in an example real case analyzed below in Section II.C (approximately 50 ms of the arcing time in Fig. 2 as compare to 250 ms in Fig. 6). For this assumption, the BDV slope leads to significantly lower number of sparks as compared to the real case analyzed in Section II.C, and thus provides more illustrative waveforms as those shown in Fig. 2.

It can be seen in Fig 2a, that the number of $n = 2$ opening operations is not sufficient to reproduce the BDV correctly, since no sparks with the negative voltage $u_d(t)$ polarity occurs at the time region of the negative BDV non-linearity $u^-_{BDV}(t)$ (see red box in Fig. 2a). Fig. 2b shows that the number of $n = 5$ opening operations gave significantly more accurate BDV reproduction (see red box in Fig. 2b), but still (in this particular case) with only one spark at the region of the negative BDV non-linearity $u^-_{BDV}(t)$. In further analyses, 360 opening disconnector operations were conducted to ensure good BDV reproduction in the region of the BDV nonlinearity.

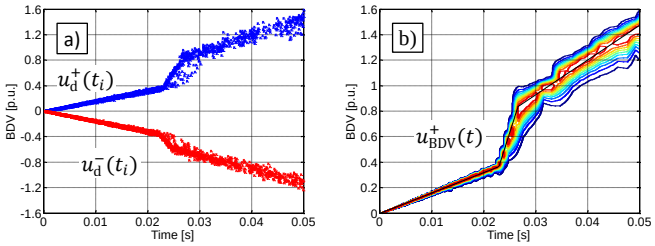

Fig. 3 a) Voltage across the disconnector contacts $u^{+/-}_d(t_i)$ calculated with Gaussian distribution, with mean value equal to the $u^{+/-}_{BDV}(t_i)$ in Fig. 2 and standard deviation equal to 5%; b) Breakdown voltage $u^+_{BDV}(t)$ (positive) determined based on simulated voltage u^+_d(positive) shown in Fig. 3a; colors in Fig. 3b are normalized to the instantaneous mean value probability (red for highest, blue for lowest values).

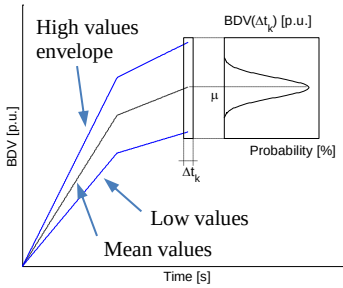

Fig. 4 Method of obtaining BDV from statistical data: probability distribution (shown in inset) fitted to the voltage u_d data in a time slice Δt_k.

The next step for the method illustration was to include the statistical behavior of the BDV assumed in Fig. 2. For this purpose, a set of 360 disconnector opening operations were simulated. For each disconnector operation, the BDV was calculated in each step of numerical simulation. For the instantaneous BDV values a Gaussian distribution was assumed with the mean values equal to the $u^+_{BDV}(t)$ and $u^-_{BDV}(t)$ lines given in Fig. 2 (for the positive and the negative $u_d(t)$ voltage values respectively), and with the standard deviation of 5%. Fig. 3a shows the resultant $u_d(t_i)$ voltage values for the time instances when the gas breakdown (sparks) occurred.

Fig. 3b shows the BDV determined based on the statistically distributed $u_d(t_i)$ voltage values shown in Fig. 3a. Fig. 4 illustrates the method used for obtaining the BDV shown in Fig. 3b. The time of the disconnector operation was divided into a number k of the time slices Δt_k. The width of Δt_k is selected so to embrace a number of sparks needed for statistical treatment. In each of the slice Δt_k the probability distribution was fitted to the statistically distributed voltage values $u_d(t_i)$ which fell into the particular slice Δt_k. As the output, the parameters of the assumed probability distribution are obtained for each of the time slice Δt_k (such as the mean μ_k and the standard deviation σ_k values in the case when the

Gaussian distribution is employed). This procedure is repeated for every time slice Δt_k, so that the discrete values of the probability distribution parameters constitutes the time-variant breakdown voltages $u_{\mathrm{BDV}}^{+/-}(t)$, which for the Gaussian distribution $\mathcal{g}$ can be written as:

$$u_{\mathrm{BDV}}^{+/-} = \mathcal{g}[\mu(t), \sigma(t)] \qquad (3)$$

It should be mentioned that different statistical distributions can be applied here. Gaussian or Weibull are the natural choices, however other approximations are also possible. In [9] the least square method is used for parameters extraction of linear model assumed.

In Fig. 3 a good agreement can be seen between the statistically distributed voltage $u_{\mathrm{d}}(t_i)$ (see Fig. 3a, as simulated according to the assumed BDV shown in Fig. 2), and the BDV fitted (see Fig. 3b, which is a statistical representation of Fig. 3a according to the procedure illustrated in Fig. 4).

C. Determination of BDV for an 1'100 kV disconnector

In this section, measurement results from development tests of an 1'100 kV disconnector are used for the BDV determination of the disconnector of an example design. The resultant BDV have been further used in the analyses presented in Section III and further referred in this paper as the *Non-linear BDV*.

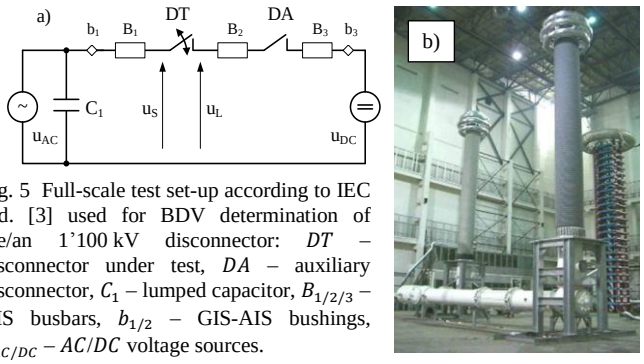

Fig. 5 Full-scale test set-up according to IEC Std. [3] used for BDV determination of the/an 1'100 kV disconnector: DT – disconnector under test, DA – auxiliary disconnector, C_1 – lumped capacitor, $B_{1/2/3}$ – GIS busbars, $b_{1/2}$ – GIS-AIS bushings, $u_{AC/DC}$ – AC/DC voltage sources.

Fig. 5 shows the development test set-up as used for the measurements. The test set-up was established according the IEC Std. [3]. The disconnector source- $u_S(t)$ and load- $u_L(t)$ side voltages were measured during the opening and closing operations of the disconnector under the test (DT). The auxiliary disconnector (DA) was used to pre-charge the GIS busbar B_2 with the TCV specified for the closing operation. The amplitude of the source side AC 50 Hz voltage was set to 1.1 p.u. (where 1 p.u. is 899 kV for the 1′100 kV rated voltage). The test procedure involved two steps. In the first step the capacitor C_1 value was selected to ensure that the first spark for the closing operation without pre-charge condition ($TCV = 0$ p.u.) leads to VFTO of at least 1.4 p.u. amplitude and less than 500 ns time to first peak. The next step involved closing operation with a given TCV condition on the busbar B_2. Approximately 100 disconnector operations were performed for each DT operation type (opening and closing), trapped charge conditions, and disconnector design.

The test set-up shown in Fig. 5 was used for testing of different disconnector designs and with different moving contact speeds. The measurement results used in this section were obtained for the disconnector with the moving contact speed of 0.39 m/s, with the relatively low BDV slope (see Fig. 7). This selection was made to provide illustrative distinction between the BDV described in this section and that the one reported in [8] and used as a benchmark in this paper. The two BDVs described are compared in Section II.D.

Fig. 6a shows the voltage $u_{\mathrm{d}}^{+/-}(t_i)$ across the contact gap of the disconnector under test DT, measured for the time instances t_i of the sparks ignitions for a number of disconnector opening operations. Fig. 6b shows the positive breakdown voltage $u_{\mathrm{BDV}}^{+}(t)$ determined based on the data shown in Fig. 6a.

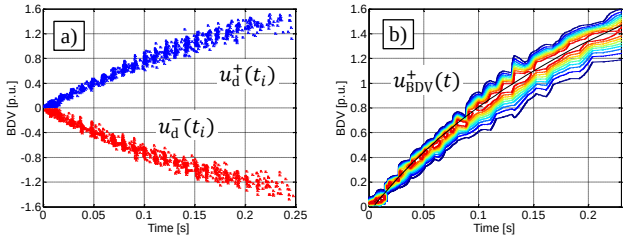

Fig. 6 a) Voltage $u_{\mathrm{d}}^{+/-}(t_i)$ measured in type-test set-up in Fig. 5 for a number of 100 disconnector opening operations; b) Breakdown voltage $u_{BDV}^{+}(t)$ (positive) determined based on measured voltage $u_{\mathrm{d}}^{+}(t_i)$ (positive) shown in Fig. 6a; colors in Fig. 6b are normalized to the instantaneous mean value probability (red for highest, blue for lowest values).

In order to verify the BDV determined as shown in Fig. 6b, the TCV distribution was simulated for a number of 360 opening operations of disconnector DT in the test set-up shown in Fig. 5. Table I shows good agreement of the mean and the standard deviation values of the Gaussian distributions of TCV between the simulation and measurement results.

TABLE I
Parameters of Gaussian distributions fitted to TCV distributions simulated (left column) and measured (right column) in test set-up in Fig. 5 for 100 disconnector opening operations; simulated TCV are based on BDV characteristics shown in Fig. 6

Simulated TCV [p.u.]	Measured TCV [p.u.]
-0.29 ± 0.07	-0.31 ± 0.10

The method presented here is equally relevant for obtaining the BDV for both opening and closing disconnector operations. The standardized type-test procedure (such as the one recommended by IEC [3]) provides all data necessary for determining and verifying the BDV characteristics of the operated disconnector. However, other test set-ups can be used as well, provided that the voltage conditions imposed by the given test set-up topology are representative for the particular GIS substation where the disconnector will eventually be applied (i.e. the maximum values of the voltage u_d across the disconnector contact gap for any disconnector operation must cover the values expected in the real conditions).

D. BDV of disconnector used in Wuhan 1100 kV station

In this section, the *Non-linear BDV* determined in Section II.C for an exemplary development design of the 1'100 kV disconnector is compared to the BDV reported in [8] for 1'100 kV disconnector tested in Wuhan station (China). From different moving contact speeds tested in the Wuhan station (as outlined in Section I), the data for the moving contact speed of 0.54 m/s was selected in this paper as providing the BDV with significantly higher slope as compared to the one obtained in Section II.C for the disconnector with moving contact speed of 0.39 m/s (see Fig. 7).

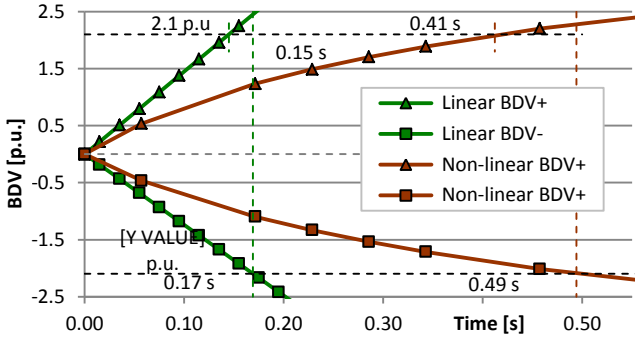

Fig. 7 BDV: determined in Section II.C (*Non-linear BDV*, in red color) and referenced in Section II.D (*Linear BDV*, in green color), as implemented in multi-spark modeling approach in Section III; maximum possible arcing times are marked for the Non-*linear BDV* and the *Linear BDV* as 0.49 s and 0.17 s respectively.

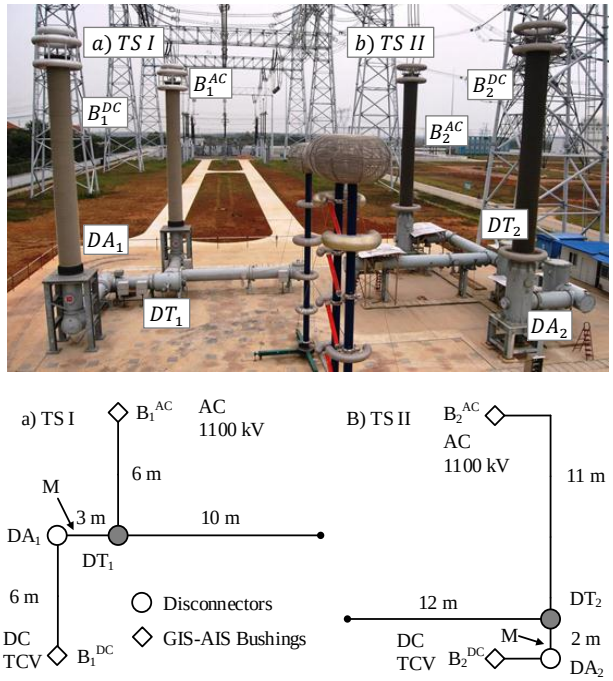

Fig. 8 Test set-ups in Wuhan 1100 kV station as reported in [8, 9] and used for analyses in Section III: *TS I* (left) and *TS II* (right); disconnector in test set-up T*S I* has moving contact speed of 0.54 m/s; lengths indicated bottom figures are assumed in Section III for simulations; measuring point *M* corresponds to *M*1 in [7].

The BDV of the Wuhan disconnector was assumed in [2], [8], [9] as having a linear characteristics. For its determination the least square approximation method was used [9]. The positive and the negative BDV slopes have been reported in [8] as $+14.5$ p.u./s and -12.4 p.u./s respectively (see Fig. 7, in green color). This BDV is used in the analyses presented in Section III and further referred in this paper as a *Linear BDV*.

Fig. 7 shows the comparison of the two BDVs: the *Non-linear BDV* as determined in Section II.C based for an exemplary development design of 1'100 kV ABB disconnector, and *Linear BDV* as reported in [8] for one of the 1100 kV disconnectors used in Wuhan station. The *Linear BDV* was assumed for the disconnector with moving contact speed of 0.54 m/s, while the *Non-Linear BDV* – for the disconnector with moving contact speed of 0.39 m/s. It can be noticed in Fig. 7 that the *Non-linear BDV* has significantly lower rate of rise time as compared to the *Linear BDV*. As a consequence, the maximum possible arcing times (i.e. for the maximum possible voltage is $|u_d| \leq 2.1$ p.u., provided that the source voltage of 1.1 p.u. is assumed) are (see Fig. 7): 0.17 s for the *Linear BDV* and 0.49 s for the *Non-Linear BDV*.

For the BDVs shown in Fig. 7, the negative breakdowns (given by u_{BDV}^{-}) occur at lower voltage $|u_d(t_i)|$ than the positive breakdowns (given by u_{BDV}^{+}), at 14.5% and 28.4% for *Linear BDV* and *Non-Linear BDV* respectively. This BDVs asymmetry is due to the asymmetry of the disconnector contact system designs. As indicated in [8], this asymmetry of the breakdown voltages u_{BDV}^{+} and u_{BDV}^{-} leads to the asymmetry of the characteristic step-wise pattern of the disconnector VFT load-side waveform as well as to the asymmetry of TCV distributions (as shown in Section III, Fig. 9-11).

The two BDVs shown in Fig. 7 (*Non-linear BDV* and *Linear BDV*) are further used in this paper for the simulations presented in Section III and Section IV.

III. Analysis of BDV Impact on VFTO Process

In order to present the applicability of the multi-spark approach with the method of the BDV determination presented in this paper, the BDVs selected in Section II (see Fig. 7) have been implemented for modeling of the disconnector operation in two full-scale 1'100 kV test set-ups as used in Wuhan station [2], [7]-[9]. The layouts of the test set-ups, together with the selected measurement results, as reported for the Wuhan station, are referenced here based on [8]. Initial simulation results presented in this section served as ABB contribution to CIGRE TB 542 [11].

A. 1100 kV test set-up in Wuhan

Fig. 8 shows the two 1100 kV test set-ups in Wuhan station [8]. They both have the same layout, but with different lengths of particular busbars and different designs of the disconnectors under test. Test set-up I (see *TS I* in Fig. 8) employs a 90°-angled disconnector (DT_1), while in test set-up II (see *TS II* in Fig. 8) a straight disconnector (DT_2) was used.

In the simulations reported below the lengths of the GIS busbars are assumed based on [8] (see Fig. 8). Other parameters of the GIS components and bushings are assumed based on the 1'100 kV components used in the test set-up shown in Fig. 5. The Wuhan test set-ups shown in Fig. 8 are similar to the standardized ones as recommended by IEC Std.

[4] (see Fig. 5), with the two differences: addition of the busducts indicated in Fig. 8 with 10 m length for *TS I* and 12 m length for *TS II*, and disregarding the capacitor C_1 (as shown in Fig. 5a).

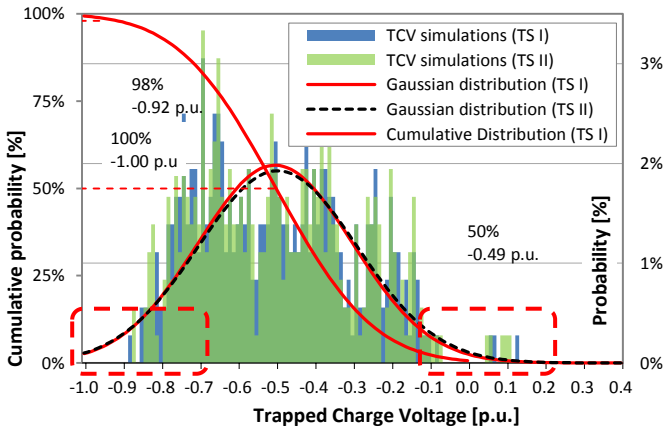

Fig. 9 TCV distributions simulated for opening operation of disconnector *DT* in test set-ups *TS I* and *TS II* (see Fig. 8), with *Linear BDV* shown in Fig. 7; moving contact speed 0.54 m/s; mean and standard deviation values are given in Table IV; quantiles of cumulative distribution (100%, 98%, and 50% are referred in Table II and Table III for calculation of VFTO during disconnector closing operation.

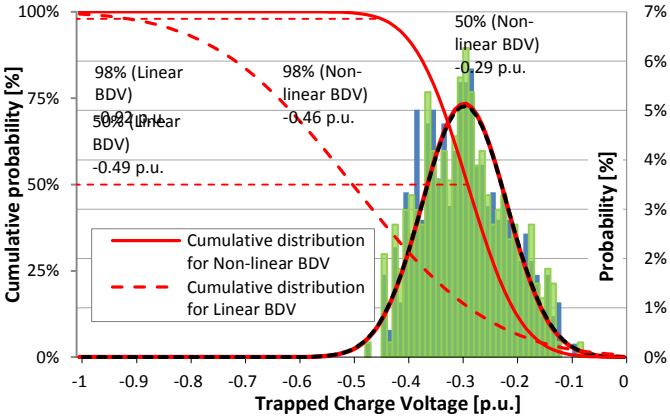

Fig. 10 TCV distributions simulated for opening operation of disconnector *DT* in test set-ups *TS I* and *TS II* (see Fig. 8), with *Non-linear BDV* shown in Fig. 7; moving contact speed 0.39 m/s; mean and standard deviation values are given in Table IV; quantiles of cumulative distributions (100%, 98%, and 50% are referred in Table II and Table III for calculation of VFTO during disconnector closing operation.

In [8] the *Linear BDV* characteristics (see Fig. 7) is reported as characterizing the disconnector DT_1 in the test set-up *TS I* (see Fig. 8). For the simulations here presented, the BDVs shown in Fig. 7 were implemented in both test set-ups, *TS I* and *TS II*. This allowed one to analyze the impact of the BDVs on the VFTO conditions (by employing different BDVs in the same test layouts) and vice versa (by employing same BDVs in different test set-up layouts). The disconnector's moving contact speeds of 0.54 m/s and 0.39 m/s were selected. The 0.54 m/s represented the lowest speed from those investigated in [2], [7]-[9], and the 0.39 m/s represented the lowest speed from those investigates in [1], [4], [6]. As such they gave the highest impact on the TCV reduction (as compared to the worst case of −1 p.u. value as recommended by IEC Std. [3]), along with the highest impact on the increase of the sparking time and the number of sparks. The disconnector opening time was assumed as 0.45 s to make sure that the maximum possible sparking time is covered (see Fig. 7).

B. Analysis of Trapped Charge Voltage distributions

Fig. 9 and Fig. 10 show TCV distributions simulated for the two test set-ups shown in Fig. 8 (*TS I* and *TS II*) with the use of two BDVs presented in Fig. 7 (*Non-linear BDV* and *Linear BDV*). Cumulative probability is scaled on the left-hand axes, while distributions of probability per window width of 0.01 p. u. is scaled on the right-hand axes.

Since the *Non-linear BDV* has lower slope as compared to the *Linear BDV* (see Fig. 7), the TCV distribution for the *Non-linear BDV* (see Fig. 10) is characterized with the lower mean and standard deviation values as compared to the TCV distribution for the *Linear BDV* (see Fig. 9). The results for the *Non-linear BDV* are thus equivalent to the disconnector with the lower moving contact speed, which is in agreement with e.g. [1]. The set of cumulative TCV distributions analyzed in [1] for different speeds of the disconnector's moving contact shown decreased mean values and slopes of cumulative TCV distributions for the lower disconnector's moving contact speeds.

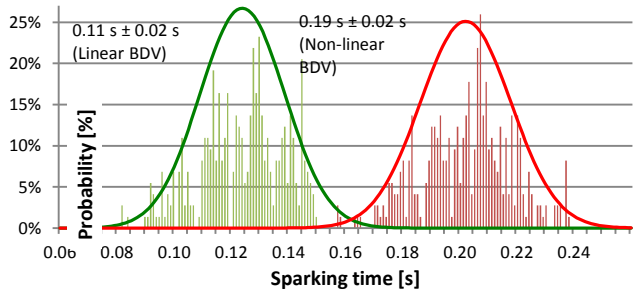

Fig. 11 Sparking time simulated for opening operation of disconnector *DT* in test set-up *TS I* (see Fig. 8a), with *Linear BDV* for moving contact speed 0.54 m/s (left-most; 0.11 s ± 0.02 s) and *Non-linear BDV* for moving contact speed 0.39 m/s (right-most; 0.19 s ± 0.02 s) shown in Fig. 7.

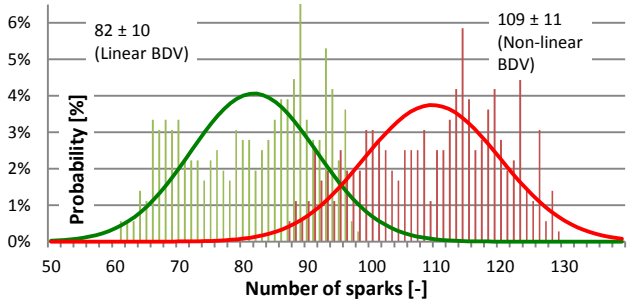

Fig. 12 Number of sparks simulated for opening operation of disconnector *DT* in test set-up *TS I* (see Fig. 8a), with *Linear BDV* for moving contact speed 0.54 m/s (82 ± 10) and *Non-linear BDV* for moving contact speed 0.39 m/s (109 ± 11) shown in Fig. 7.

C. Sparking time and number of sparks for opening operation

For the opening operation, sparking time is defined as the time interval between the time instance of the contacts parting and the time instance of the last spark occurrence in the process of the disconnector opening operation. Fig. 11 and Fig. 12 show the sparking time and the total number of sparks

respectively, simulated for the Wuhan test set-up *TS I* (see Fig. 8a) with the two BDVs shown in Fig. 7. As expected, higher sparking time ($0.19\ \text{s} \pm 0.02\ \text{s}$ versus $0.11\ \text{s} \pm 0.02\ \text{s}$) and higher number of sparks (109 ± 11 versus $82\ \pm 10$) are observed for the *Non-linear BDV* (disconnector with lower moving contact speed) as compared to the *Linear BDV* (disconnector with higher moving contact speed).

D. VFTO for closing operation

VFTO for the disconnector closing operation depends on the TCV which remains on the disconnector load side after the preceding opening operation is completed. The most severe conditions are for the TCV equal to -1.0 p.u. This 'worst-case' TCV value is used in the standardized procedure of the disconnector type-testing as recommended in IEC Std. [3]. In practice, the TCV strongly depends on the BDV, which in turn is specific to particular disconnector design. As a consequence, for some of the designs, the 'worst-case' TCV value of -1 p.u. is highly unlikely. In such cases, by assuming the TCV value for the specific disconnector design, more realistic VFTO can be estimated.

TABLE II
VFTO simulated for closing operation of disconnector *DT* in **test set-up *TS I*** (see Fig. 8a, measuring point *M*), with *Non-linear BDV* and *Linear BDV* shown in Fig. 7, for different TCV values read from Fig. 9 (for *linear BDV*) and Fig 10 (for *Non-linear BDV*)

	Non-linear BDV		**Linear BDV**	
TCV [%]	**TCV [p.u.]**	**VFTO [p.u.] (δ [%])**	**TCV [p.u.]**	**VFTO [p.u.] (δ [%])**
100	-1.00	2.34 (100.0)	-1.00	2.34 (100.0)
98	-0.46	1.97 (84.4)	-0.92	2.28 (97.4)
50	-0.29	1.86 (79.5)	-0.49	1.99 (85.2)

TABLE III
VFTO simulated for closing operation of disconnector *DT* in **test set-up *TS II*** (see Fig. 8b, measuring point *M*), with *Non-linear BDV* and *Linear BDV* shown in Fig. 7, for different TCV values read from Fig. 9 (for *linear BDV*) and Fig 10 (for *Non-linear BDV*)

	Non-linear BDV		**Linear BDV**	
TCV [%]	**TCV [p.u.]**	**VFTO [p.u.] (δ [%])**	**TCV [p.u.]**	**VFTO [p.u.] (δ [%])**
100	-1.00	2.42 (100.0)	-1.00	2.42 (100.0)
98	-0.46	2.03 (84.0)	-0.92	2.37 (97.9)
50	-0.29	1.54 (63.9)	-0.49	2.06 (85.1)

Table II and Table III show the VFTOs calculated in two test set-ups *TS I* and *TS II* (see Fig. 8) for three values of TCV (quintile: 100%, 98%, and 50%) as shown in Fig. 9 and Fig. 10. Both BDVs shown in Fig. 7 were implemented (*Non-linear BDV* and *Linear BDV*). The VFTOs were calculated for the measuring point *M* (see Fig. 8), corresponding to the measuring point M_1 as reported in [7] (see Fig. 1 in [7]).

It can be noticed in Table II and Table III, that the VFTO depends on the test set-up layout (which is not the case for the TCV distributions as shown in Fig. 9 and Fig. 10, where the layout dependence is negligible). In both test set-ups, the VFTO strongly depends on the TCV value used for the simulations. Since the TCV values are lower for the *Non-linear BDV* as compare to the *Linear BDV*, the VFTOs are lower for the *Non-Linear BDV* as well.

IV. Experimental Validation of Selected Results

Fig. 13 presents the TCV distribution measured in the test set-up *TS I* (see Fig. 8a) and referenced here from [8]. Table IV summarizes the mean and the standard deviation values of the Gaussian distributions fitted to the simulation results shown in Fig. 9 and Fig. 10.

It can be noticed that the TCV distributions strongly depend on the BDV characteristics employed (see Fig. 9 vs. Fig. 10), whereas the impact of the particular test set-up layout is negligible (see Fig. 9 and Fig. 10). Agreement in terms of mean and standard deviation parameters can qualitatively be seen between the simulation results obtained here with the use of the *Linear BDV* (see Fig. 9 and Table IV), and the measurement results obtained in the Wuhan station [8] (see Fig. 13). The discrepancies marked with dashed boxes in Fig. 9 can be explained by the simplified, linear approximation of the BDV, which was used here based on [8] (where the BDV was determined with the simplified, linear approximation). The agreement between the simulation and the measurement results (see Fig. 9 vs. Fig. 13) indicates that the implementation of the *Linear BDV* characteristics in the multi-spark approach here employed is correct.

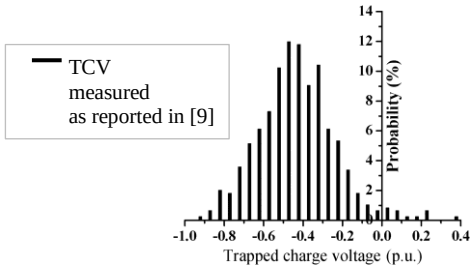

Fig. 13 TCV distribution measured for opening operation of disconnector *DT* in test set-up *TS I* (see Fig. 8a); moving contact speed 0.54 m/s; this figure is reproduced here from [7] (see Fig. 9 in [7]).

TABLE IV
Parameters of Gaussian distributions fitted to TCV distributions shown in Fig. 9 and Fig. 10, simulated for opening operation of disconnector *DT* in test set-ups *TS I* and *TS II* (see Fig. 8), with *Non-linear BDV* and *Linear BDV* shown in Fig. 7; simulation results for *Linear BDV* are in good agreement with the measurement results shown in Fig. 13

	Linear BDV (see Fig. 7, in green)	**Non-linear BDV (see Fig. 7, in red)**
Test set-up *TS I* (see Fig. 8a)	-0.501 ± 0.201	-0.2929 ± 0.0777
Test set-up *TS II* (see Fig. 8b)	-0.495 ± 0.207	-0.2927 ± 0.0784

In [7] the VFTO peak value of 2.20 p.u. was reported as measured for the disconnector with $0.54\ \text{m/s}$ moving contact speed tested in test set-up *TS I* shown in Fig. 8a with $TCV\ =$

−1 p.u. This value is in a good agreement with the simulated VFTO peak value of 2.34 p.u. as obtained here for the *Linear BDV* in the test set-up *TS I* (see Table II).

V. Conclusions

Development of Gas-Insulated Switchgear (GIS) is currently taking place towards EHV and UHV rated voltages, reaching the level of 1'100 kV in the ongoing projects in China. In the paper an approach for determination of Breakdown Voltage Characteristics (BDV) of 1'100 kV disconnector was employed for modeling of Very Fast Transient Overvoltages (VFTO) generated during operation of the GIS disconnector. Applicability of the BDV determination approach was shown with respect to the GIS design aspects.

Examples of simulation results have been presented to provide outline of the BDV determination method. Comparison between simulation and measurement results obtained or referenced based on 1'100 kV test set-ups provided the approach validation based on full-scale measurements.

As presented throughout the paper, analyses based on the BDV obtained for a real disconnector gave a comprehensive insight into the VFTO conditions in the GIS, and thus can be used to support design and product development stages of the new GIS components and substations. It is important for design work that the BDV employed is obtained from development tests on a real disconnector. Moreover, by knowing the actual BDV as related to the specific disconnector design, the most severe VFTO conditions can be calculated, as well as the worst case scenario in terms of the TCV can be defined.

The paper presented the impact of the difference in the BDV on certain parameters of the VFTO generation process. The results indicate that the real BDV is needed to be applied for design work, since differences in the results (see Table IV) are significant.

VI. References

[1] M. Szewczyk, W. Piasecki, M. Stosur, U. Riechert, and J. Kostovic, "Impact of disconnector design on very fast transient overvoltages in gas-insulated UHV switchgear," presented at the *17th Int. Symp. High Voltage Eng. (ISH)*, Hannover, Germany, Aug. 22–26, 2011.

[2] S. Yinbiao, H. Bin, L. Ji-Ming, Ch. Weijiang, B. Liangeng, X. Zutao, and Ch. Guoqiang, "Influence of the Switching Speed of the Disconnector on Very Fast Transient Overvoltage," *IEEE Trans. Power Delivery*, vol. 28, no. 4, pp. 2080-2084, Oct. 2013.

[3] *High-Voltage Switchgear and Controlgear—Part 102: Alternating Current Disconnectors and Earthing Switches*, IEC 62271-102.

[4] U. Riechert, M. Bösch, M. Szewczyk, W. Piasecki, J. Smajic, A. Shoory, S. Burow, and S. Tenbohlen, "Mitigation of very fast transient overvoltages in gas insulated UHV substations," in *Proc. CIGRE*, 2012.

[5] W. Holaus, U. Krüsi, D. Sologuren, U. Riechert, and M. Keller, "Testing of GIS components at 1000 kV rated voltage," in *Proc. CIGRE*, 2008.

[6] U. Riechert, U. Krüsi, D. Sologuren-Sanchez, "Very Fast Transient Overvoltages during Switching of Bus-Charging Currents by 1100 kV Disconnector," in *Proc. CIGRE*, 2010.

[7] Y. Shu, W. Chen, Z. Li, M. Dai, Ch. Li, W. Liu, and X. Yan, "Experimental Research on Very-Fast Transient Overvoltage in 1100-kV Gas-Insulated Switchgear," *IEEE Trans. Power Delivery*, vol. 28, no. 1, pp. 458-466, Jan. 2013.

[8] Y. Gongchang, L. Weidong, Ch. Weijiang, G. Yonggang, and L. Zhibing, "Development of Full Frequency Bandwidth Measurement of VFTO in UHV GIS," *IEEE Trans. Power Delivery*, vol. 28, no. 4, pp. 2550-2557, Oct. 2013.

[9] W. Chen, H. Wang, B. Han, L. Wang, G. Ma, G. Yue, Z. Li, and H. Hu, "Study on influence of Disconnector Characteristics on Very Fast Transient Overvoltage in 1100 kV Gas-Insulated Switchgear," to be published.

[10] S. A. Boggs, F. Y. Chu, N. Fujimoto, A. Krenicky, A. Plessl, and D. Schlicht, "Disconnect switch induced transients and trapped charge in gas-insulated substations," *IEEE Trans. Power App. Syst.*, vol. PAS-101, no. 10, pp. 3593–3602, Oct. 1982.

[11] Working Group C4.306, Insulation Coordination for UHV AC Systems, *CIGRE Technical Brochure 542*, June 2013

[12] *High-Voltage Switchgear and Controlgear – Part 203: Gas-Insulated Metal-enclosed Switchgear for Rated Voltages Above 52 kV*, IEC Standard 62271-203, Nov. 2003.

VII. Biographies

Marcin Szewczyk (M'2012–SM'2014), born in Koszalin, Poland, received his M.Sc. and Ph.D. degrees in Electrical Engineering from Warsaw University of Technology, Warsaw, Poland, in 2000 and 2009 respectively. He was Assistant Professor at Warsaw University of Technology. Since 2010 he is a Researcher with ABB Corporate Research in Cracow, Poland. His research is mainly in the field of power system analyses and advanced simulations, power products, transients analyses and transients mitigation, insulation coordination, 3D modeling and simulations of electromagnetic fields, modeling of magnetic materials for transient analyses, modeling of Vacuum Circuit Breakers. Dr. Szewczyk is a member of IEEE and Polish Society for Theoretical and Applied Electrical Engineering (ABB Corporate Research, Starowiślna 13A, 31-038 Krakow, Poland, E-mail: marcin.szewczyk@pl.abb.com).

Maciej Kuniewski (Student'11–M'14), born in Kraków, Poland, in 1986. He received his Ph.D. in Electrical Engineering in 2013 from AGH University of Science and Technology in Kraków. He is working as research assistant at AGH in Electrical Engineering and Electrical Power Engineering Faculty. His fields of studies are High Voltage Engineering, transients in power system, overvoltage protection, computer simulations. Maciej Kuniewski is member of IEEE and CIGRE.

Wojciech Piasecki was born in Poland on May 15,1966. He received the M.Sc. degree in electronics from the University of Science and Technology, in Kraków Poland, Poland, and the Ph.D. degree from the Jagiellonian University, Kraków. He has been working for many years in electromagnetic and electrical phenomena, including high-frequency and nonlinear modeling of electrical equipment. Currently, he is a Researcher with the Corporate Research Center in Kraków. His main research concentrates around transient network phenomena analysis.

Marek Florkowski (M'97-SM'08) received the M.S. and Ph.D. degrees in electronics from AGH University of Science and Technology in Kraków in 1990 and 1994, respectively. From 1990 to 1992 he was employed at ABB Corporate Research Center in Baden-Dättwil. In 2009 he obtained habilitation. He is currently responsible for ABB Corporate Research in Krakow, Poland. A member of CIGRE, and APEE. He is chair of the Technical Committee on Diagnostics of the IEEE Dielectrics and Electrical Insulation Society.

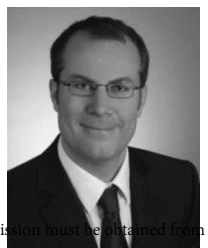

Ueli Straumann (M'10–SM'12) was born in Aarau, Switzerland, in 1975. He received the Ph.D. degree in electrical engineering from ETH Zurich, Zurich,

Switzerland, in 2007. Since then, he has been a Lecturer of High Voltage Engineering, ETH Zurich. After being Senior Assistant at the High Voltage Laboratory of ETH Zurich between 2007 and 2012, he became Senior and Principal Engineer at the GIS R&D of ABB Switzerland Ltd.